

Molecular determinants of the interactions between proteins and ssDNA

Garima Mishra and Yaakov Levy¹

Department of Structural Biology, Weizmann Institute of Science, Rehovot 76100, Israel

Edited by G. Marius Clore, National Institutes of Health, Bethesda, MD, and approved March 6, 2015 (received for review August 24, 2014)

ssDNA binding proteins (SSBs) protect ssDNA from chemical and enzymatic assault that can derail DNA processing machinery. Complexes between SSBs and ssDNA are often highly stable, but predicting their structures is challenging, mostly because of the inherent flexibility of ssDNA and the geometric and energetic complexity of the interfaces that it forms. Here, we report a newly developed coarse-grained model to predict the structure of SSB–ssDNA complexes. The model is successfully applied to predict the binding modes of six SSBs with ssDNA strands of lengths of 6–65 nt. In addition to charge–charge interactions (which are often central to governing protein interactions with nucleic acids by means of electrostatic complementarity), an essential energetic term to predict SSB–ssDNA complexes is the interactions between aromatic residues and DNA bases. For some systems, flexibility is required from not only the ssDNA but also, the SSB to allow it to undergo conformational changes and the penetration of the ssDNA into its binding pocket. The association mechanisms can be quite varied, and in several cases, they involve the ssDNA sliding along the protein surface. The binding mechanism suggests that coarse-grained models are appropriate to study the motion of SSBs along ssDNA, which is expected to be central to the function carried out by the SSBs.

ssDNA | protein–DNA interaction | coarse-grained model

Double-stranded DNA (dsDNA) contains all of the genetic information necessary for proper cellular functioning. The dsDNA unwinds to form ssDNA. This intermediate structure enables the stored information to be accessed; however, it is thermodynamically less stable than dsDNA, and consequently, it spontaneously forms duplex secondary structures (which inhibit subsequent DNA-processing reactions) and is more susceptible to environmental hazards (which can damage the genome). A solution to this problem adopted across many different domains of life comes from specialized ssDNA binding proteins (SSBs) that bind, protect, and stabilize the ssDNA structures required for essential genomic processes and therefore, enable these processes to proceed (1–3).

Most SSBs share a common structural motif called the *oligosaccharide/oligonucleotide* binding (OB) fold, which consists of a five-stranded β -sheet arranged as a β -barrel capped by a single α -helix to bind ssDNA (4). However, this common structural motif itself has widely varying characteristics. For example, the OB folds in different proteins can range in length from 70 to 150 aa, and the loops connecting the β -sheets that are responsible for binding specificities vary in sequence, length, and conformation (5). Furthermore, it is quite difficult to detect the OB fold domains based on sequence similarity alone, because most proteins containing this structural motif share a low degree (5–25%) of sequence similarity (4).

Most bacterial SSBs form a homotetramer and contain one OB fold per polypeptide, with each such fold capable of binding to ssDNA (6). Binding involves the ssDNA wrapping around the homotetramer, although bacterial SSBs exhibit considerable variability in their association. In contrast to bacterial SSBs, eukaryotic SSBs generally function as a heterotrimer consisting of six OB folds distributed among three subunits; however, only four of these OB folds are involved in binding to ssDNA (7), which results

in an extended arrangement for the protein–ssDNA complex. Telomere end binding proteins, which safeguard the vulnerable telomere 3' end of ssDNA, also use different numbers of OB folds to bind with ssDNA (8). These proteins show high sequence specificities for their respective telomeric sequences, and this sequence preference may be linked to their function as telomeres (8–10). Furthermore, very few SSBs have been structurally characterized as using the K homology domain (three α -helices packed against a three-stranded β -sheet) and RNA recognition motif domains (8) to form a complex with ssDNA.

The complexes between SSBs and ssDNA are often very thermodynamically stable (11, 12), and their binding relies on the electrostatic interactions between the negatively charged phosphates of the ssDNA and the complementary positively charged residues [lysine (K), arginine (R), or histidine] of the SSBs. The same electrostatic attraction is also required for protein binding to dsDNA (13), with SSBs differentiating ssDNA from its dsDNA competitor on the basis of the intrinsic properties of each, in that dsDNA is significantly less flexible in regards to the spacing and positioning of its negative charges than ssDNA. In addition to the electrostatic interaction, detailed structural studies of crystal complexes of ssDNA–SSB complexes suggest that the aromatic residues tryptophan (W), phenylalanine (F), tyrosine (Y), and histidine (H) also play an important role in ssDNA–SSB binding (Fig. S1).

Although strong electrostatic binding of SSBs to ssDNA is necessary to stabilize the latter, the transient role of SSBs in DNA metabolic processes also requires the recycling of SSBs (i.e., their dissociation from and reassociation with ssDNA) as well as their repositioning within ssDNA complexes (14). Recent studies using single-molecule fluorescence resonance energy transfer have endeavored to shed light on the dynamic activity of different types of SSBs, which were earlier thought to form inert

Significance

The association between proteins and DNA, which is essential for many biological functions, very often produces high-affinity complexes, in which the protein retains the ability to move along the DNA. These features are common to the binding of proteins either to dsDNA or ssDNA. Although protein–dsDNA interactions have been well-explored, research in the field of protein–ssDNA complexes is still in its infancy, particularly on the theoretical and computational fronts. The major factors that complicate the prediction of protein–ssDNA compared with protein–dsDNA complexes are the much greater flexibility of ssDNA compared with dsDNA and the larger heterogeneity of their interfaces. Here, we begin to fill this gap by developing a minimalist computational model to predict the protein–ssDNA binding mode.

Author contributions: G.M. and Y.L. designed research, performed research, analyzed data, and wrote the paper.

The authors declare no conflict of interest.

This article is a PNAS Direct Submission.

¹To whom correspondence should be addressed. Email: koby.levy@weizmann.ac.il.

This article contains supporting information online at www.pnas.org/lookup/suppl/doi:10.1073/pnas.1416355112/-DCSupplemental.

complexes with ssDNAs. These studies have shown that the *Escherichia coli* SSB functions as a sliding platform that migrates on ssDNA (10, 15), whereas a homodimeric bacterial SSB from *Thermus thermophilus* is able to diffuse spontaneously along ssDNA (16). It was reported that the diffusion coefficient of the *E. coli* SSB along ssDNA is similar to that of transcription factors along dsDNA (17). Efficient sliding dynamics on ssDNA were recently elegantly shown for replication protein A (RPA) (18).

SSBs are not the only groups binding to and moving along ssDNA. For example, the complex between the protection of telomeres protein 1 (Pot1) and thiamine pyrophosphate protein 1 (TPP1; i.e., the Pot1–TPP1 complex) slides back and forth on telomeric DNA (19, 20). Similarly, RPA can bind very tightly to an ssDNA and dissociate rapidly when other SSBs are present in solution (20). Unlike studies (10, 15, 16, 19) that were performed on an infinitely dilute solution, the findings of the study in ref. 20 apply to a wide range of conditions. Thus, the study of SSB diffusion elucidates the mechanism used by SSBs to recruit other SSB-interacting enzymes onto ssDNA and give due access to the genome substrate for subsequent processing.

As described above, the experimental community has given considerable attention to probing the different aspects of SSB–ssDNA complexes. However, almost no efforts have been made on the theoretical front. To address this gap, this paper aims to develop a universal model that can predict the crystal complex of ssDNA with SSBs coming from different domains of life, which can be further extended to study other properties of these complexes in future studies.

Results and Discussion

Role of Electrostatic and Aromatic Interactions in ssDNA–SSB Binding.

The power of the developed coarse-grained model to predict the structures of SSB–ssDNA is presented in Fig. 1. Fig. 1 shows the probability of the occurrence of different states of the SSB–ssDNA complex as characterized by structural parameters that measure the similarity of the predicted ssDNA–SSB interface to the interface in the X-ray or NMR structures. For a refined comparison, the aromatic and positively charged residues that comprise the interface were split into two patches, quantified as D_1 and D_2 (Fig. S1). Areas closer to the (0,0) intersection between the D_1 and D_2 axes represent structures that more closely resemble the interface in the crystal structure. The free energy landscape for formation of each of six studied complexes where the interface between the SSB and ssDNA is modeled by electrostatic and aromatic interactions reflects that, in all six cases, near-native conformations with low values of D_1 and D_2 are reasonably populated (Fig. 1, *Left*). The importance of both the electrostatic and aromatic interactions for the specificity and stability of the interface is illustrated by plotting the interfacial aromatic residues for each system together with the electrostatic potential (Fig. 1, *Right*). We note that coarse-grained models that included only electrostatic or aromatic interactions yielded poor results, with the latter profoundly inferior to the former (Figs. S2 and S3). In the following paragraphs, we focus on the binding of several different SSBs with ssDNA in the presence of these two interactions and examine their role in binding.

The binding of the *Schizosaccharomyces pombe* Pot1p complex with homopolymeric ssDNA using both electrostatic and aromatic interactions is shown in Fig. 1A. Although the ssDNA sometimes found the correct protein binding pocket in the presence of electrostatic interactions only (Fig. S2), the resulting complex deviated from the crystal structure. By contrast, when aromatic interactions between the aromatic amino acids of Pot1p and the ssDNA bases were included together with the electrostatic interactions (as in Fig. 1A), the structure of the complex tended toward that of the crystal structure. It is noteworthy that the experimental crystal structure for the same complex was obtained with sequence-specific ssDNA (9), which can engage in base stacking. Although we did not consider sequence effects in ssDNA here, we

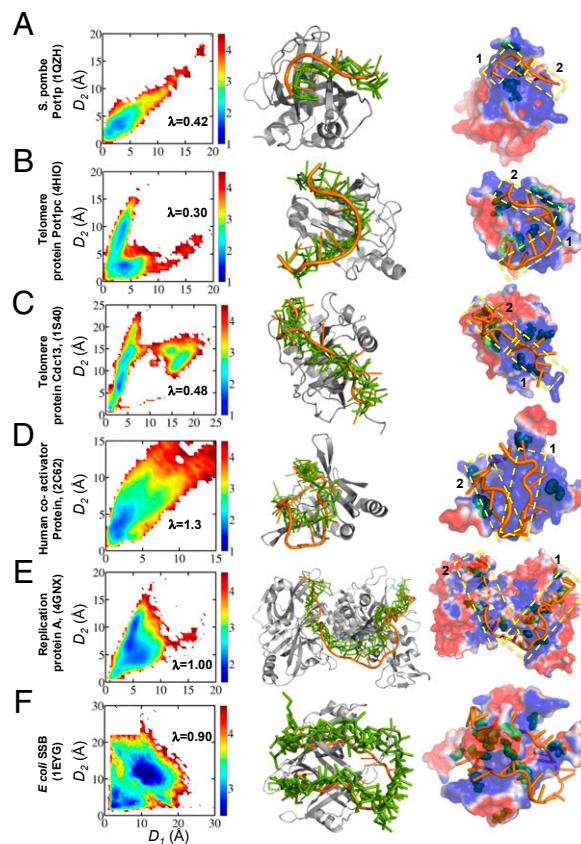


Fig. 1. Predicted conformational ensemble for six different SSB–ssDNA complexes (A–F). The similarity measure (D) quantifies the overall structural similarity between the predicted binding interface in the ssDNA–protein complex and the interface observed in the crystal structure (a lower value of D corresponds to a greater degree of similarity with the crystal structure, with a value of zero representing 100% concordance). For a detailed structural comparison, each SSB–ssDNA interface was divided into two regions (schematically marked by rectangles in *Right*; accurate definition in *S1 Methods*) that were assessed separately as D_1 and D_2 . The color bar shows the free energy of the different binding states of the complex in the presence of both electrostatic and aromatic interactions. Sample structures corresponding to high probability maps (i.e., the lowest values of D_1 and D_2) are shown in *Center*. In these structures, the ssDNA is shown in green, and for comparison, the conformation of the ssDNA in the corresponding crystal structure is shown in orange (the proteins are shown in gray). *Right* shows the interfacial aromatic residues for each system together with the electrostatic potential. The ssDNA is shown in orange. The aromatic residues (F, Y, W, and H) that interact with the ssDNA are shown as green spheres. Additional aromatic residues that are exposed to the solvent can be found on the protein surface but are not shown. In many cases, the aromatic residues are located in negatively charged regions. The values of λ (the ratio between the total electrostatic and aromatic energies of each SSB–ssDNA complex) are shown in the maps in *Left*. Additional molecular and structural details of each of the six complexes can be found in [Table S1](#).

nevertheless found very good agreement between the conformation of the ssDNA and that of the crystal structure, which strongly suggests that aromatic interactions play a role.

The similarity measures map for the telomeric protein Pot1pc with 9-mer ssDNA shows large variations in D_1 and D_2 with different probabilities in the presence of electrostatic interactions only (Fig. S2). The structure shown in Fig. S3 corresponds to the highest probability patch in the map; a similar structure also occurred at the opposite end of the binding groove with a low probability of occurrence. These extended structures occurring at either end of the Pot1pc binding groove depended solely on the electrostatic interaction. As aromatic interactions

in which nucleotide 22 interacts with site I, such as in the crystal structure.

Fig. 3B shows that correct binding of the ssDNA with site II occurred right after site I was occupied, indicating that sliding from site I to site II was relatively fast. The sliding of the ssDNA continued from site II toward site III with formation of the correct interface at time step $\sim 5.0 \times 10^6$ that proceeded immediately toward site IV. The sliding of the ssDNA, as suggested by this trajectory, did not take place at the same pace between the sites, presumably because of the different conformations that the ssDNA acquired at each site (e.g., their aromatic and electrostatic composition).

The structures shown in Fig. 3, *Right* are snapshots of four different conformations selected from the trajectory and correspond to the time frames marked by arrows 1–4 in Fig. 3, *Left*. We point out that, although site I constituted the initial association event, it is possible to find cases in which other sites engaged first. The probability of the initial binding occurring first with one of the sites depends on their molecular properties, and therefore, they are not necessarily equivalent.

A similar mechanism for back and forth sliding of ssDNA was also observed for Pot1pC (Fig. 4) by following the value of $|r_{\text{model}} - r_{\text{crystal}}|$ and the nucleotide identity to a selected site in two different trajectories. Although the ssDNA interacts with each of these sites at the beginning of the simulation (reflected by the immediate decrease of the value of $|r_{\text{model}} - r_{\text{crystal}}|$), the identity of the nucleotide interacting with the sites changes throughout the simulation. The sliding of the ssDNA is also shown pictorially in Fig. 4 at three different instances in time for each trajectory. It is clear from the electrostatic map of Pot1pC (Fig. 1) that there are two potential pathways through which ssDNA can enter into the binding pocket of the protein, unlike the situation for the telomere protein Cdc13, where the negatively charged electrostatic region on one side blocks the path of the ssDNA (Fig. 1). Fig. 4A shows the sliding behavior of ssDNA from one side, and

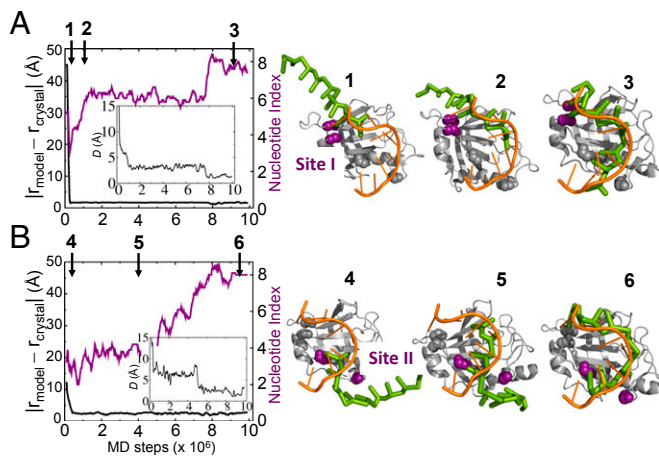


Fig. 4. Mechanism of ssDNA binding to Pot1pC. The association is illustrated by two different trajectories. The trajectories illustrate binding first to site (A) I or (B) II. Sites I and II are defined as the centers of mass of residues W72 and H109 and W27 and R59, respectively, and they are shown at three different time points as indicated by the arrows. The ssDNA can enter into the binding pocket of the protein from either of two sides. The initial binding to either site is followed by substantial sliding relative to the corresponding site. A pictorial representation of ssDNA sliding during its binding to the Pot1pC protein is shown for each trajectory by three snapshots (marked by 1–3 and 4–6 for the trajectories shown in A and B, respectively). *Insets* show the time evolution of the total similarity measure D for each binding trajectory, illustrating that complete binding is achieved only toward the end of the simulation ($D \sim 2 \text{ \AA}$).

it also remains true if the ssDNA enters from the opposite side (Fig. 4B). Fig. 4, *Insets* show the time evolution of the similarity measure D , which indicates that the correct and more complete interface between the 9-nt ssDNA and Pot1pC is achieved toward the end of the simulation.

Conclusions

The complexes formed between proteins and ssDNA are not only fundamentally different from those formed between proteins and dsDNA but also, more difficult to predict. Two major factors complicate the prediction of SSB–ssDNA complexes compared with protein–dsDNA complexes: the much greater flexibility and consequent lack of definitive structure of ssDNA compared with dsDNA and the larger heterogeneity of the SSB–ssDNA interface. These two complexities are related to each other. The disordered nature of ssDNA enables it to interact with proteins mostly through the phosphate groups, which may attract charged side chains, or the bases, which may interact with aromatic side chains, with a consequent increase in interface heterogeneity. As a result of these complicating factors, SSB–ssDNA complexes have received little attention from theoreticians.

To address this gap, this paper aimed to develop a transferable model to predict the crystal complex of ssDNA with SSBs coming from different domains of life. The important molecular components of the coarse-grained model for predicting the SSB–ssDNA complexes were electrostatic and aromatic interactions between the charged and aromatic amino acids and between the DNA phosphates and bases, respectively. In addition to incorporating the inherent flexibility of ssDNA, the model incorporated the flexibility of the proteins to improve the binding predictions for some complexes. More elaborate models that include, for example, ion condensation may better describe the conformational dynamics of ssDNA and the interface that they may form with SSBs. Despite the massive computer resources that are required for these such models, they may allow researchers to explore distinct association modes at different salt conditions, which was observed experimentally for RPA (27) and *E. coli* SSB (25, 26). Our coarse-grained model successfully predicted the binding modes of six complexes of different sizes (132–694 aa and 6–65 nt). Thus, the model produces useful results using more widely available computing resources. The model can be further extended to study other properties of these complexes (such as the sliding of SSB along ssDNA) and readily combined with experimental research in future studies.

Methods

We used a coarse-grained model to explore the binding of ssDNA to SSBs at the molecular level. The model represents each protein residue by two beads placed at the $C\alpha$ - and $C\beta$ -positions. Beads representing charged amino acids (K, R, H, D, and E) have a charge at the $C\beta$ -position. The protein is simulated by a native topology-based model and uses the Lennard–Jones (L–J) potential to represent native contact interactions. Overall, we followed an approach to protein modeling similar to that described in refs. 28 and 29. The internal energy of the protein is designated by E_{prot} . In addition to the inherent flexibility of the proteins in the coarse-grained model, which is dictated by the density of the native contacts, we incorporated enhanced flexibility for regions characterized by high B factors or residues with no electron density.

The ssDNA was modeled by three beads per nucleotide (representing the phosphate, sugar, and base) that were positioned at the geometric center of each represented group. The phosphate bead in the model bears a negative charge. The model potential for ssDNA used in our study, which follows other models (30–32), is given by $E_{\text{ssDNA}} = E_{\text{ssDNA}}^{\text{Bond}} + E_{\text{ssDNA}}^{\text{Angle}} + E_{\text{ssDNA}}^{\text{Dihedral}} + E_{\text{ssDNA}}^{\text{Base pairing}} + E_{\text{ssDNA}}^{\text{Stacking}} + E_{\text{ssDNA}}^{\text{Repulsion}}$. The first three terms dictate the flexibility of the ssDNA backbone, whereas the last three terms govern the global structure of the ssDNA. Two major interactions involved in the stability of ssDNA are base pairing and stacking interactions. Often, a homopolymeric ssDNA (poly T or poly C) is used in experimental studies of SSB–ssDNA complexes, which prohibits the formation of base pairing. However, the formation of stacks still remains possible depending on the type of nucleotides comprising the ssDNA. Therefore, to consider the effect of base stacking in ssDNA, we added

a short-range attraction between consecutive bases of ssDNA in the form of the L-J potential, with an energetic contribution of ε_{B-B} (SI Methods and Fig. S6).

The interaction potential between a protein amino acid (AA) and ssDNA nucleotides arises from three contributions: (i) the electrostatic interaction between the C β -bead representing a charged amino acid (K, R, H, D, and E) and the negatively charged phosphate of ssDNA, (ii) the aromatic stacking interaction between the C β -bead representing an aromatic amino acid (W, F, Y, and H) and an ssDNA base, and (iii) the repulsive interactions between other beads of the protein and ssDNA. Thus, $E_{\text{prot-ssDNA}} = E_{\text{prot-ssDNA}}^{\text{Elec}} + E_{\text{prot-ssDNA}}^{\text{Aromatic}} + E_{\text{prot-ssDNA}}^{\text{Repulsion}}$. The electrostatic interactions acting between all of the charged beads in the system are modeled by the Debye-Hückel potential (29). The aromatic interaction, similar to base stacking, is modeled by the L-J potential, with a base-aromatic amino acid interaction strength of ε_{B-AA} . The parameter $\varepsilon_{B-AA} = 0$ for all of the nonaromatic amino acids, and $\varepsilon_{B-AA} > 0$ only for aromatic amino acids (W, F, Y, and H). Trp has a large surface area compared with other aromatic residues (F, Y, and H), and hence, ε_{T-W} may make a larger contribution than ε_{T-F} , ε_{T-Y} , and ε_{T-H} when the aromatic amino acids form stacks with the bases of ssDNA. Given the coarse-grained nature of the model, we calibrated the relative strengths of the electrostatic and aromatic contributions and selected the following values: $\varepsilon_{T-F} = \varepsilon_{T-Y} = \varepsilon_{T-H} = 2$ and $\varepsilon_{T-W} = 3$ (Fig. S7).

Using the total potential energy ($E_{\text{prot}} + E_{\text{ssDNA}} + E_{\text{prot-ssDNA}}$) of the SSB-ssDNA complex, the dynamics of the protein and ssDNA were simulated using Langevin dynamics. The ssDNA-SSB complex was studied at a salt concentration of 0.01 M using the dielectric constant of water and a temperature at which the bound state of the complex is more populated. The model was initially tested for its ability to maintain the native structure of all of the complexes when we used it as the initial input for simulation. We started the predictive simulation by placing a free ssDNA (of the same length as the ssDNA in the corresponding crystal structure) at different positions. A total of 600 simulations for each system was collected, analyzing a total of 6×10^4 conformations.

We then calculated a structural similarity parameter (D) to quantify the degree of deviation of the simulation from the known crystal structure. To

obtain the similarity parameter, we first identified the interfacial residues as the C β -bead of residues (either positively charged or aromatic amino acids) with distance that was less than 9 Å from any ssDNA phosphate or any base in the crystal structure. The simulation to crystal structure similarity parameter is calculated by $D = N_{\text{prot}}^{-1} N_{\text{ssDNA}}^{-1} \sum_i \sum_j \sum_k \sum_l \sum_m \sum_n \sum_o \sum_p \sum_q \sum_r \sum_s \sum_t \sum_u \sum_v \sum_w \sum_x \sum_y \sum_z \sum_{i,j} \sum_{i,k} \sum_{i,l} \sum_{i,m} \sum_{i,n} \sum_{i,o} \sum_{i,p} \sum_{i,q} \sum_{i,r} \sum_{i,s} \sum_{i,t} \sum_{i,u} \sum_{i,v} \sum_{i,w} \sum_{i,x} \sum_{i,y} \sum_{i,z} \sum_{j,k} \sum_{j,l} \sum_{j,m} \sum_{j,n} \sum_{j,o} \sum_{j,p} \sum_{j,q} \sum_{j,r} \sum_{j,s} \sum_{j,t} \sum_{j,u} \sum_{j,v} \sum_{j,w} \sum_{j,x} \sum_{j,y} \sum_{j,z} \sum_{k,l} \sum_{k,m} \sum_{k,n} \sum_{k,o} \sum_{k,p} \sum_{k,q} \sum_{k,r} \sum_{k,s} \sum_{k,t} \sum_{k,u} \sum_{k,v} \sum_{k,w} \sum_{k,x} \sum_{k,y} \sum_{k,z} \sum_{l,m} \sum_{l,n} \sum_{l,o} \sum_{l,p} \sum_{l,q} \sum_{l,r} \sum_{l,s} \sum_{l,t} \sum_{l,u} \sum_{l,v} \sum_{l,w} \sum_{l,x} \sum_{l,y} \sum_{l,z} \sum_{m,n} \sum_{m,o} \sum_{m,p} \sum_{m,q} \sum_{m,r} \sum_{m,s} \sum_{m,t} \sum_{m,u} \sum_{m,v} \sum_{m,w} \sum_{m,x} \sum_{m,y} \sum_{m,z} \sum_{n,o} \sum_{n,p} \sum_{n,q} \sum_{n,r} \sum_{n,s} \sum_{n,t} \sum_{n,u} \sum_{n,v} \sum_{n,w} \sum_{n,x} \sum_{n,y} \sum_{n,z} \sum_{o,p} \sum_{o,q} \sum_{o,r} \sum_{o,s} \sum_{o,t} \sum_{o,u} \sum_{o,v} \sum_{o,w} \sum_{o,x} \sum_{o,y} \sum_{o,z} \sum_{p,q} \sum_{p,r} \sum_{p,s} \sum_{p,t} \sum_{p,u} \sum_{p,v} \sum_{p,w} \sum_{p,x} \sum_{p,y} \sum_{p,z} \sum_{q,r} \sum_{q,s} \sum_{q,t} \sum_{q,u} \sum_{q,v} \sum_{q,w} \sum_{q,x} \sum_{q,y} \sum_{q,z} \sum_{r,s} \sum_{r,t} \sum_{r,u} \sum_{r,v} \sum_{r,w} \sum_{r,x} \sum_{r,y} \sum_{r,z} \sum_{s,t} \sum_{s,u} \sum_{s,v} \sum_{s,w} \sum_{s,x} \sum_{s,y} \sum_{s,z} \sum_{t,u} \sum_{t,v} \sum_{t,w} \sum_{t,x} \sum_{t,y} \sum_{t,z} \sum_{u,v} \sum_{u,w} \sum_{u,x} \sum_{u,y} \sum_{u,z} \sum_{v,w} \sum_{v,x} \sum_{v,y} \sum_{v,z} \sum_{w,x} \sum_{w,y} \sum_{w,z} \sum_{x,y} \sum_{x,z} \sum_{y,z}$. Here, i and j are the i th bead of the selected C β bead of the protein and the j th bead of the ssDNA, respectively, and thus, r_{ij} and r_{ij}^0 are the pairwise distances between those beads in the simulated and the crystal structure, respectively. The pairwise distances were calculated either between each selected aromatic amino acids and all of the B beads of the ssDNA or between each of the selected charged amino acids and all of the phosphate beads of the ssDNA. N_{prot} is the total number of selected interfacial amino acid residues (positively charged or aromatic), and N_{ssDNA} is the number of nucleotides in the length of ssDNA examined. Thus, the term D quantifies the overall conformational similarity between the predicted binding interface in the ssDNA-protein complex and the crystal structure, with a D value = 0 indicating 100% conformational similarity. To obtain a finer structural quantification of the interface, we divided the selected interfacial residues into two groups that cover two different regions of the interface. We then calculated two order parameters, D_1 and D_2 , each characterizing the accuracy of the prediction for the corresponding region of the interface (Fig. S1).

It is important to note that we used information from the crystal structure solely to model the protein, whereas transferable potentials were used to model the structure and energetics of both the ssDNA and the interface protein-ssDNA. Thus, our model does not include any bias toward the specific binding mode. In our study, we investigated six different SSB-ssDNA complexes (Table S1). A detailed description is in SI Methods.

ACKNOWLEDGMENTS. We are grateful to Peter Stern for performing atomistic simulations of the SSB-ssDNA complexes. This work was supported by the Kimmelman Center for Macromolecular Assemblies and the Minerva Foundation, with funding from the Federal German Ministry for Education and Research. Y.L. is The Morton and Gladys Pickman professional chair in Structural Biology.

- Lohman TM, Ferrari ME (1994) Escherichia coli single-stranded DNA-binding protein: Multiple DNA-binding modes and cooperativities. *Annu Rev Biochem* 63:527-570.
- Wold MS (1997) Replication protein A: A heterotrimeric, single-stranded DNA-binding protein required for eukaryotic DNA metabolism. *Annu Rev Biochem* 66:61-92.
- Pestryakov PE, Lavrik OI (2008) Mechanisms of single-stranded DNA-binding protein functioning in cellular DNA metabolism. *Biochemistry (Mosc)* 73(13):1388-1404.
- Theobald DL, Mitton-Fry RM, Wuttke DS (2003) Nucleic acid recognition by OB-fold proteins. *Annu Rev Biophys Biomol Struct* 32:115-133.
- Flynn JM, Levchenko I, Sauer RT, Baker TA (2004) Modulating substrate choice: The SspB adaptor delivers a regulator of the extracytoplasmic-stress response to the AAA+ protease ClpXP for degradation. *Genes Dev* 18(18):2292-2301.
- Raghunathan S, Kozlov AG, Lohman TM, Waksman G (2000) Structure of the DNA binding domain of E. coli SSB bound to ssDNA. *Nat Struct Biol* 7(8):648-652.
- Fan J, Pavletich NP (2012) Structure and conformational change of a replication protein A heterotrimer bound to ssDNA. *Genes Dev* 26(20):2337-2347.
- Dickey TH, Altschuler SE, Wuttke DS (2013) Single-stranded DNA-binding proteins: Multiple domains for multiple functions. *Structure* 21(7):1074-1084.
- Lei M, Podell ER, Cech TR (2004) Structure of human POT1 bound to telomeric single-stranded DNA provides a model for chromosome end-protection. *Nat Struct Mol Biol* 11(12):1223-1229.
- Roy R, Kozlov AG, Lohman TM, Ha T (2009) SSB protein diffusion on single-stranded DNA stimulates RecA filament formation. *Nature* 461(7267):1092-1097.
- Kozlov AG, Lohman TM (1998) Calorimetric studies of E. coli SSB protein-single-stranded DNA interactions. Effects of monovalent salts on binding enthalpy. *J Mol Biol* 278(5):999-1014.
- Kozlov AG, Lohman TM (2006) Effects of monovalent anions on a temperature-dependent heat capacity change for Escherichia coli SSB tetramer binding to single-stranded DNA. *Biochemistry* 45(16):5190-5205.
- Marcovitz A, Levy Y (2011) Frustration in protein-DNA binding influences conformational switching and target search kinetics. *Proc Natl Acad Sci USA* 108(44):17957-17962.
- Ha T, Kozlov AG, Lohman TM (2012) Single-molecule views of protein movement on single-stranded DNA. *Annu Rev Biophys* 41:295-319.
- Zhou R, et al. (2011) SSB functions as a sliding platform that migrates on DNA via reptation. *Cell* 146(2):222-232.
- Zhang J, Zhou R, Inoue J, Mikawa T, Ha T (2014) Single molecule analysis of Thermus thermophilus SSB protein dynamics on single-stranded DNA. *Nucleic Acids Res* 42(6):3821-3832.
- Lee KS, et al. (2014) Ultrafast redistribution of E. coli SSB along long single-stranded DNA via intersegment transfer. *J Mol Biol* 426(13):2413-2421.
- Nguyen B, et al. (2014) Diffusion of human replication protein A along single-stranded DNA. *J Mol Biol* 426(19):3246-3261.
- Hwang H, Buncher N, Opreko PL, Myong S (2012) POT1-TPP1 regulates telomeric overhang structural dynamics. *Structure* 20(11):1872-1880.
- Gibb B, et al. (2014) Concentration-dependent exchange of replication protein A on single-stranded DNA revealed by single-molecule imaging. *PLoS ONE* 9(2):e87922.
- Mitton-Fry RM, Anderson EM, Theobald DL, Glustrom LW, Wuttke DS (2004) Structural basis for telomeric single-stranded DNA recognition by yeast Cdc13. *J Mol Biol* 338(2):241-255.
- Tinland B, Pluen A, Sturm J, Weill G (1997) Persistence length of single-stranded DNA. *Macromolecules* 30(19):5763-5765.
- Murphy MC, Rasnik I, Cheng W, Lohman TM, Ha T (2004) Probing single-stranded DNA conformational flexibility using fluorescence spectroscopy. *Biophys J* 86(4):2530-2537.
- Werten S, Moras D (2006) A global transcription cofactor bound to juxtaposed strands of unwound DNA. *Nat Struct Mol Biol* 13(2):181-182.
- Lohman TM, Overman LB (1985) Two binding modes in Escherichia coli single strand binding protein-single stranded DNA complexes. Modulation by NaCl concentration. *J Biol Chem* 260(6):3594-3603.
- Bujalowski W, Lohman TM (1986) Escherichia coli single-strand binding protein forms multiple, distinct complexes with single-stranded DNA. *Biochemistry* 25(24):7799-7802.
- Kumaran S, Kozlov AG, Lohman TM (2006) Saccharomyces cerevisiae replication protein A binds to single-stranded DNA in multiple salt-dependent modes. *Biochemistry* 45(39):11958-11973.
- Levy Y, Wolynes PG, Onuchic JN (2004) Protein topology determines binding mechanism. *Proc Natl Acad Sci USA* 101(2):511-516.
- Givaty O, Levy Y (2009) Protein sliding along DNA: Dynamics and structural characterization. *J Mol Biol* 385(4):1087-1097.
- Ouldrige TE, Louis AA, Doye JP (2011) Structural, mechanical, and thermodynamic properties of a coarse-grained DNA model. *J Chem Phys* 134(8):085101.
- Morriss-Andrews A, Rottler J, Plotkin SS (2010) A systematically coarse-grained model for DNA and its predictions for persistence length, stacking, twist, and chirality. *J Chem Phys* 132(3):035105.
- Freeman GS, Hinckley DM, de Pablo JJ (2011) A coarse-grain three-site-per-nucleotide model for DNA with explicit ions. *J Chem Phys* 135(16):165104.